

## Supplementary Information - Four-wave-mixing microscopy reveals non-colocalisation between gold nanoparticles and fluorophore conjugates inside cells

Naya Giannakopoulou,<sup>1</sup> Joseph B. Williams,<sup>1</sup> Paul R. Moody,<sup>2</sup> Edward J. Sayers,<sup>2</sup>  
Johannes P. Magnusson,<sup>3</sup> Iestyn Pope,<sup>1</sup> Lukas Payne,<sup>1</sup> Cameron Alexander,<sup>3</sup>  
Arwyn T. Jones,<sup>2</sup> Wolfgang Langbein,<sup>4</sup> Peter Watson,<sup>1</sup> and Paola Borri<sup>1,\*</sup>

<sup>1</sup>*School of Biosciences, Cardiff University,  
Museum Avenue, Cardiff CF10 3AX, UK*

<sup>2</sup>*School of Pharmacy, Cardiff University,  
Museum Avenue, Cardiff CF10 3NB, UK*

<sup>3</sup>*School of Pharmacy, University of Nottingham, Nottingham NG72RD, UK*

<sup>4</sup>*School of Physics and Astronomy, Cardiff University,  
The Parade, Cardiff CF24 3AA, UK*

---

\* borri@cf.ac.uk

## CONTENTS

S1. Cross correlation coefficient $r_P$	2
S2. Wide-field epi-fluorescence in cells	6
S3. HeLa cells loaded with 15nmAuNP-PC-Tf(A488)	8
S4. Autofluorescence in 3T3-L1 cells	12
S5. Autofluorescence of fused silica and glass coverslips	14
S6. Full field of view images of extinction and wide-field fluorescence microscopy	15
S7. Analysis of fluorescence quenching	20
References	23

### S1. CROSS CORRELATION COEFFICIENT $r_P$

When mapping two images acquired from different instruments solely on the basis of the cell contour in DIC and reflection microscopy, without using fiducials, it is possible that a small rotation and translation adjustment is needed to correctly overlay the images. To account for that, we calculated the image cross correlation coefficient  $r_P$  (also known as Pearson's coefficient [1]) as a function of relative translation  $(\Delta x, \Delta y)$  and rotation  $(\Delta \theta)$  coordinates. The corresponding cross-correlation images  $r_P(\Delta x, \Delta y, \Delta \theta)$  are shown in Fig. S1, S2 and S3 for the results on HeLa cells loaded with the 40nmAuNP-SA-Bi-Tf(A647), 10nmAuNP-SA(A488)-Bi-Tf(A647) and 15nmAuNP-PC-Tf(A488) construct shown in Fig. 1, Fig. 2, and Fig. 4 respectively.

Cross-correlation images as a function of relative translation were also calculated for the results shown in Fig. 3 and Fig. 6 regarding AuNPs deposited onto a glass surface, correlatively imaged by extinction and wide-field fluorescence microscope. The corresponding cross-correlation images  $r_P(\Delta x, \Delta y)$  are shown in Fig. S4 and Fig. S5.

The cross-correlation was calculated using a MATLAB script, according to the following formula of the Pearson's coefficient [1]:

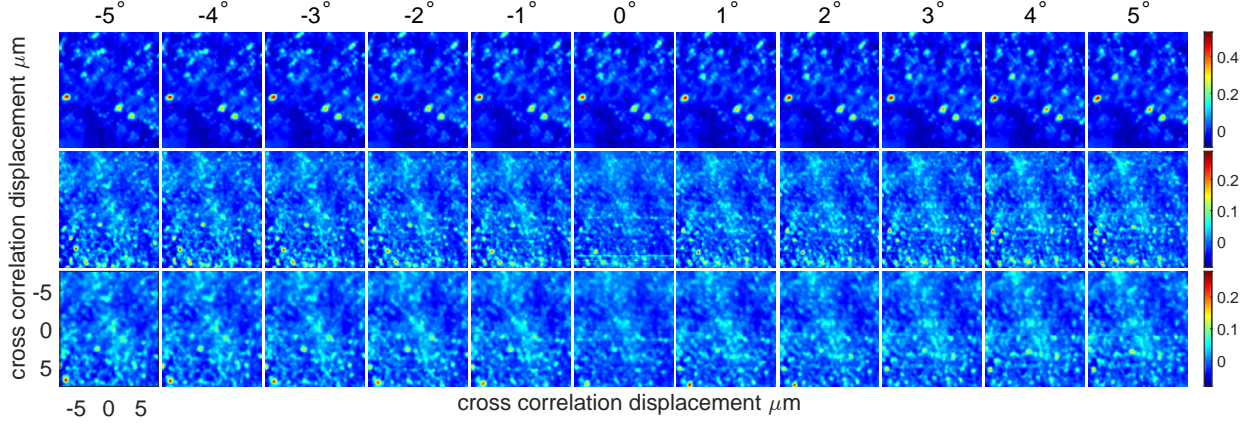


FIG. S1. Cross correlation coefficient  $r_P$  as a function of relative translation  $(\Delta x, \Delta y)$  and rotation  $(\Delta \theta)$  coordinates for the results on HeLa cells loaded with the 40nmAuNP-SA-Bi-Tf(A647) construct shown in Fig. 1. Row 1 corresponds to region A, Row 2 to region B, Row 3 to region C in Fig. 1. For each region, 11 tiles are plotted corresponding to a series of rotation angles from  $-5^\circ$  to  $+5^\circ$  in  $1^\circ$  step, as indicated.

$$r_P = \frac{\sum_i (A_i - \bar{A}) \times (B_i - \bar{B})}{\sqrt{[\sum_i (A_i - \bar{A})^2] \times [\sum_i (B_i - \bar{B})^2]}} \quad (1)$$

where  $A_i$  and  $B_i$  are the intensities in pixel  $i$  in the two images A and B to be cross-correlated, and  $\bar{A}$  and  $\bar{B}$  are the average intensity of image A and B. Upon shift and rotation of one image relative to the other, the summation runs over the overlap area between A and B.

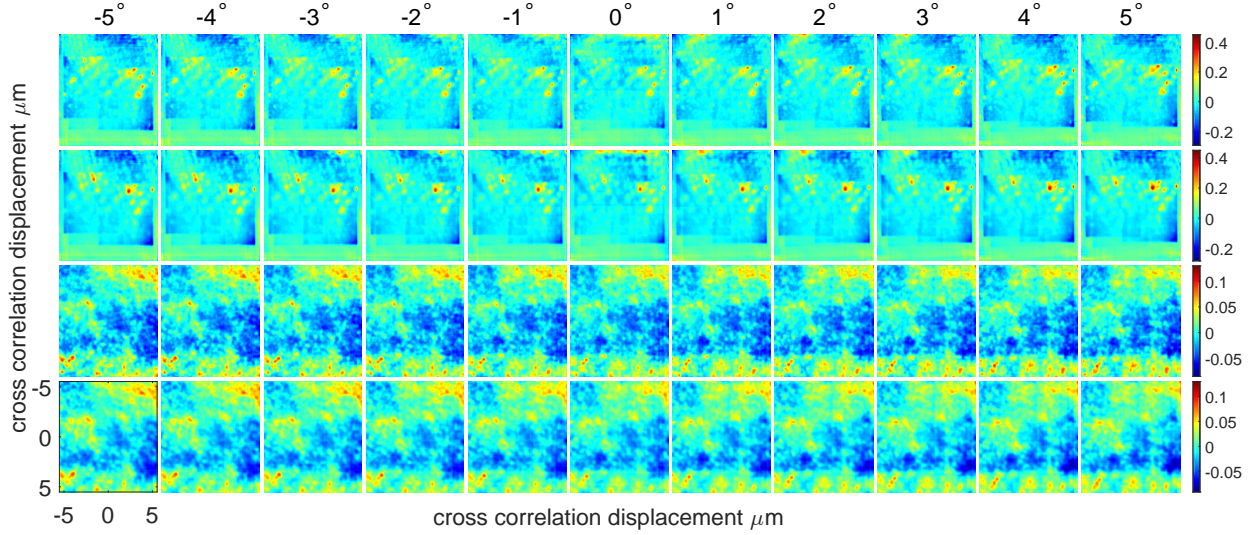


FIG. S2. Cross correlation coefficient  $r_P$  as a function of relative translation ( $\Delta x, \Delta y$ ) and rotation ( $\Delta \theta$ ) coordinates for the results on HeLa cells loaded with the 10nmAuNP-SA(A488)-Bi-Tf(A647) construct shown in Fig. 2. First and second row refer to region A in Fig. 2 (the first row refers to the A488 fluorophore, the second row to the A647). The third and fourth row refer to region B (Third row: A488; Fourth row: A647). For each region, 11 tiles are plotted corresponding to a series of rotation angles from  $-5^\circ$  to  $+5^\circ$  in  $1^\circ$  step, as indicated.

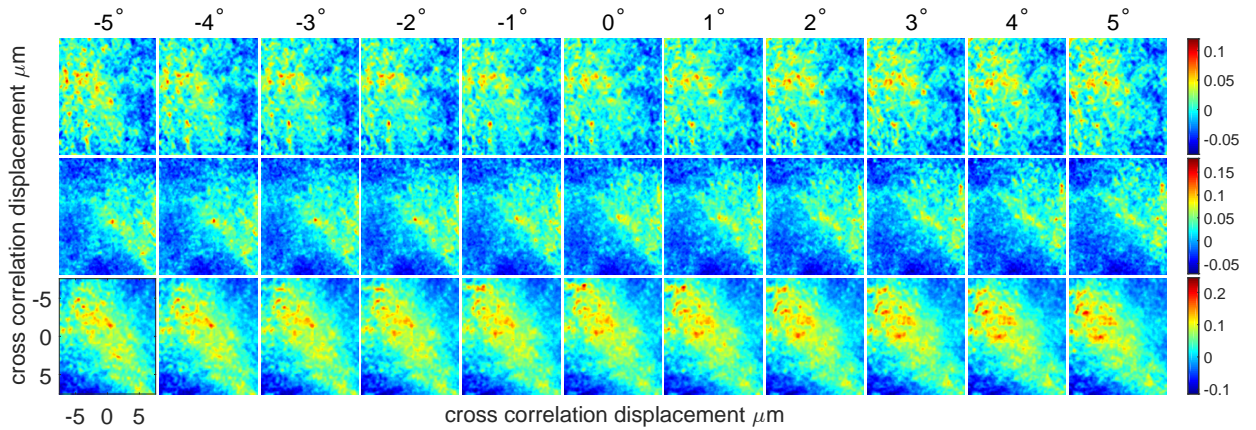


FIG. S3. Cross correlation coefficient  $r_P$  as a function of relative translation ( $\Delta x, \Delta y$ ) and rotation ( $\Delta \theta$ ) coordinates for the results on HeLa cells loaded with the 15nmAuNP-PC-Tf(A488) construct shown in Fig. 4. Row 1 corresponds to region A in Fig. 4, Row 2 to region B, Row 3 to region C. For each region, 11 tiles are plotted corresponding to a series of rotation angles from  $-5^\circ$  to  $+5^\circ$  in  $1^\circ$  step, as indicated.

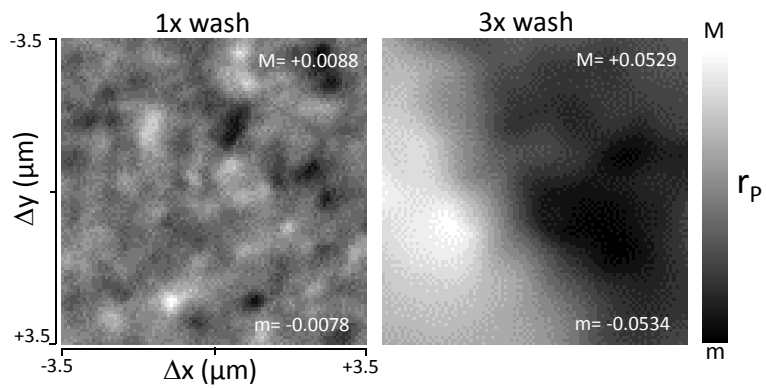


FIG. S4. Cross correlation coefficient  $r_P$  as a function of relative translation  $(\Delta x, \Delta y)$  coordinates for the 10nmAuNP-SA(A488) construct shown in Fig. 3.

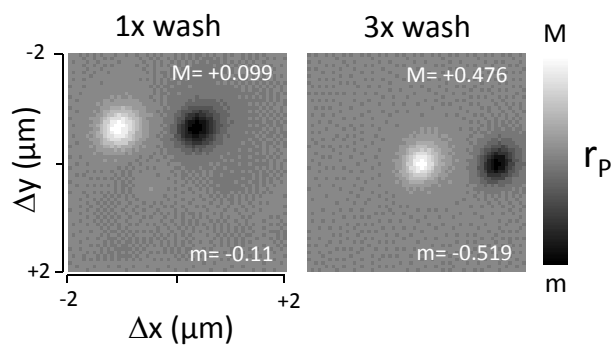


FIG. S5. Cross correlation coefficient  $r_P$  as a function of relative translation  $(\Delta x, \Delta y)$  coordinates for the 20nmAuNP-PC-Ab(A647) construct shown in Fig. 6.

## S2. WIDE-FIELD EPI-FLUORESCENCE IN CELLS

In the case of HeLa cells loaded with the 10nmAuNP-SA(A488)-Bi-Tf(A647), wide-field fluorescence images of the Alexa488 and Alexa647 fluorophores performed prior to FWM acquisition show a high density of these labels. Notably, the spatial distribution of the Alexa488 correlates well with that of Alexa647 fluorophore, with a Pearson's coefficient of 0.913. This is shown in Fig. S6. The linear relationship between the intensities in the two images and the corresponding Pearson's coefficient are calculated using JACoP, a well documented toolbox for subcellular colocalization analysis under ImageJ [1]. The Pearson's coefficient as a function the relative translation coordinates  $(\Delta x, \Delta y)$  calculated as discussed in Section S1 is shown for comparison in the inset of Fig. S6b. It exhibits a clear maximum centred at  $\Delta x = \Delta y = 0$  corresponding to the value of 0.913.

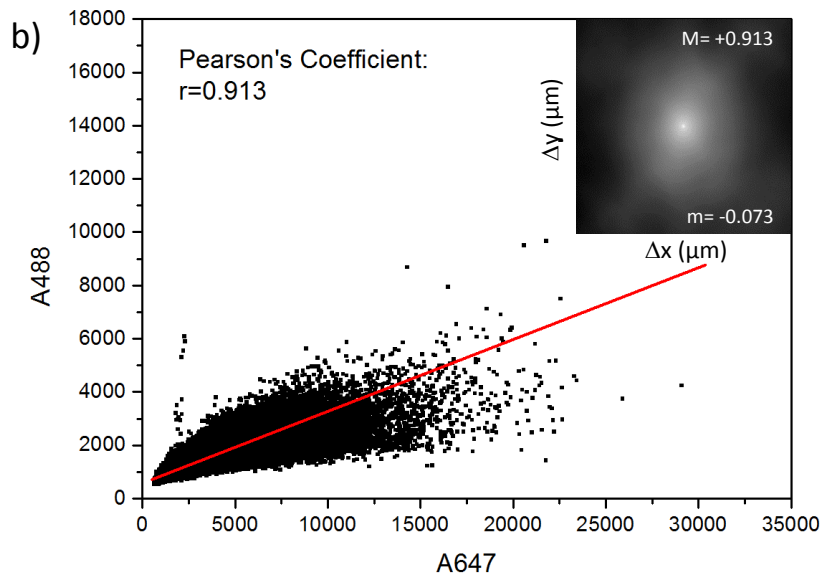
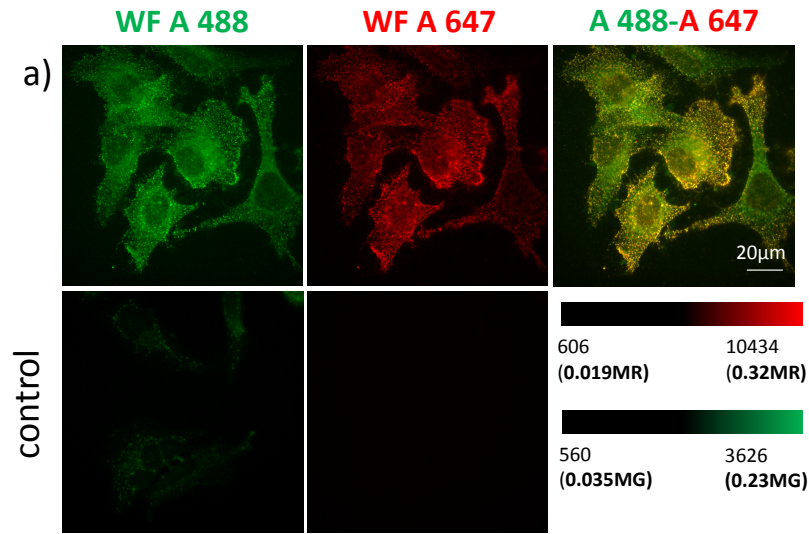


FIG. S6. a) Wide-field fluorescence images of the Alexa488 and Alexa647 labels on HeLa cells loaded with the 10nmAuNP-SA(A488)-Bi-Tf(A647), indicated as WF A488 and WF A647 respectively. A large area overview is shown, including the regions in Fig.2. WF A488 (green) and WF A647 (red) images are scaled to maximize color overlap in the corresponding overlay (green intensity from 0.035 to 0.23 of its maximum MG, red intensity from 0.019 to 0.32 of its maximum MR; values are also given on a 16bit range). b) Scatter plot showing the intensity of a given pixel in the WF A647 image used as the x-coordinate and the intensity of the corresponding pixel in the WF A488 image as the y-coordinate. The linear relationship between the intensities in the two images (red line) and the corresponding Pearson's coefficient are shown, calculated using JACoP (see text). The inset shows the Pearson's coefficient on a grey scale from  $m$  to  $M$ , as a function of relative translation coordinates  $(\Delta x, \Delta y)$  over a range of  $70 \mu\text{m} \times 70 \mu\text{m}$  centred at zero.

### S3. HELA CELLS LOADED WITH 15NMAUNP-PC-TF(A488)

In the main paper in Fig. 4 examples of reflection, FWM and confocal fluorescence images are shown on HeLa cells incubated with the 15nmAuNP-PC-Tf(A488) construct. For clarity, considering the high NP density in this case, FWM images are shown at a single  $x, y$  plane at the glass substrate interface, identified using the reflected field amplitude outside the cell regions which is highest at this interface as a function of  $z$ . Maximum intensity projections through a  $5 \mu\text{m}$  thickness are shown in Fig.S7.

A large area overview of the confocal fluorescence image of the Alexa488 label is shown in Fig. S8 as maximum intensity projection over a  $6.4 \mu\text{m}$   $z$ -stack in  $250 \text{ nm}$   $z$  steps, scaled from 0 to its maximum intensity, after applying background subtraction as explained in the Materials and Methods section of the paper.

Additional data were acquired on HeLa cells incubated with 15nmAuNP-PC-Tf(A488) at a nanoparticle density of  $4.23 \times 10^{12}$  AuNP/mL (1 in 30 dilution of the stock concentration) and fixed without washing the NPs after 2 hours incubation. Hence, compared to the results shown in the main paper in Fig. 4, cells had been loaded with NPs at a lower density, and several particles are expected to be present outside the cells. Images on these sample were acquired using a different confocal microscope than the one described in the main manuscript. Briefly, a Zeiss LSM 880 upright confocal microscope was used comprising a fully-motorised (x, y, z) Zeiss Axio Imager. The 488 nm laser line was used to excite the Alexa488 label, with a plan apochromat 63x, 1.4 NA oil objectives. Images were acquired with a 4-fold line averaging at  $30 \mu\text{s}$  line time ( $0.5 \mu\text{s}$  pixel time), with a 3D voxel size of  $132 \text{ nm} \times 132 \text{ nm} \times 335 \text{ nm}$ . Fig.S9 shows confocal fluorescence and FWM imaging on these cells. To aid the correlative imaging, fluorescent polystyrene beads of 200 nm diameter had been added as fiducials in this sample, since these beads can be seen in the reflection modality simultaneously acquired with FWM (see yellow arrows in Fig.S9b). When comparing the FWM image with the confocal fluorescence image in Fig.S9a, we can clearly observe AuNPs both inside and outside the cell via their FWM signal, however there is no fluorescence above the background that correlates with the AuNPs. Notably, there is a significant autofluorescence emission inside the cell which dominates the fluorescence detection.

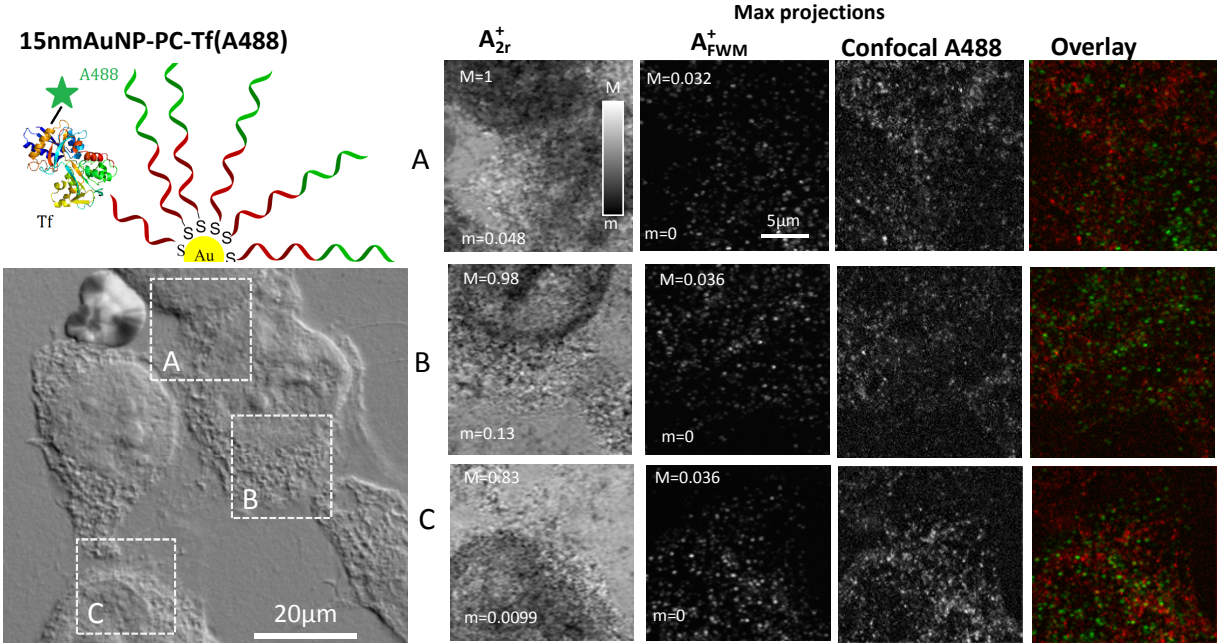


FIG. S7. Top left: Sketch of the AuNP construct. Bottom left: Fixed HeLa cells that have internalized 15nmAuNP-PC-Tf(A488) imaged by differential interference contrast microscopy. Right: Reflection amplitude ( $A_{2r}^+$ ), FWM amplitude ( $A_{FWM}^+$ ) and confocal fluorescence microscopy of the regions highlighted in DIC. FWM was acquired with a pump-probe delay time of 0.5 ps, pump (probe) power at the sample of  $31 \mu\text{W}$  ( $16 \mu\text{W}$ ), 2 ms-pixel dwell time, pixel size in plane of 94 nm and z stacks over  $5 \mu\text{m}$  in 250 nm z steps. FWM is shown as maximum intensity projections over a  $5 \mu\text{m}$  thickness, while the reflection is on a single x,y plane. Grey scales are linear from m to M for field amplitudes, as indicated (M=1 corresponds to 10mV rms detected by the lock-in). Confocal fluorescence of the Alexa488 is shown as maximum intensity projections over a  $6.4 \mu\text{m}$  z-stack in 250 nm z steps, scaled from 0 to its maximum intensity (after applying background subtraction). Overlay: fluorescence (red), FWM amplitude (green).

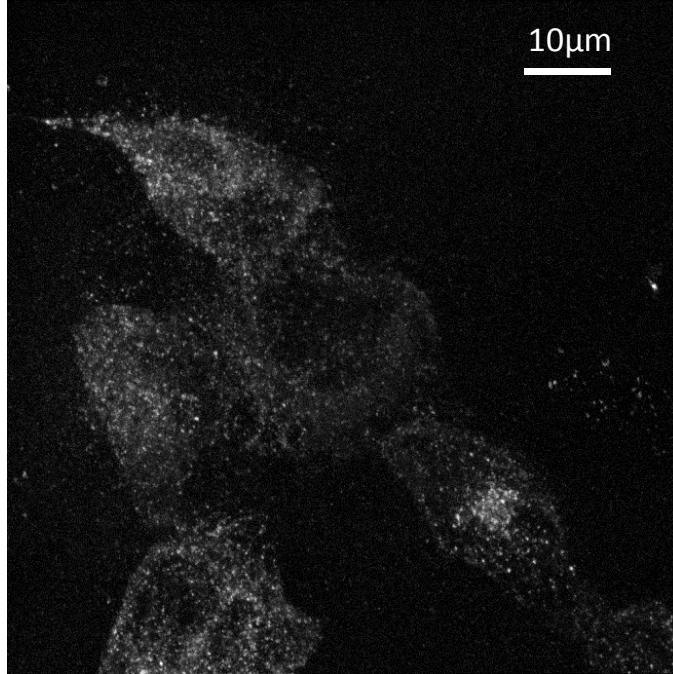


FIG. S8. Large-area confocal fluorescence image of the Alexa488, shown as maximum intensity projections over a  $6.4\ \mu\text{m}$  z-stack in 250 nm z steps, scaled from 0 to its maximum intensity (after applying background subtraction, see Materials and Methods section of the main paper).

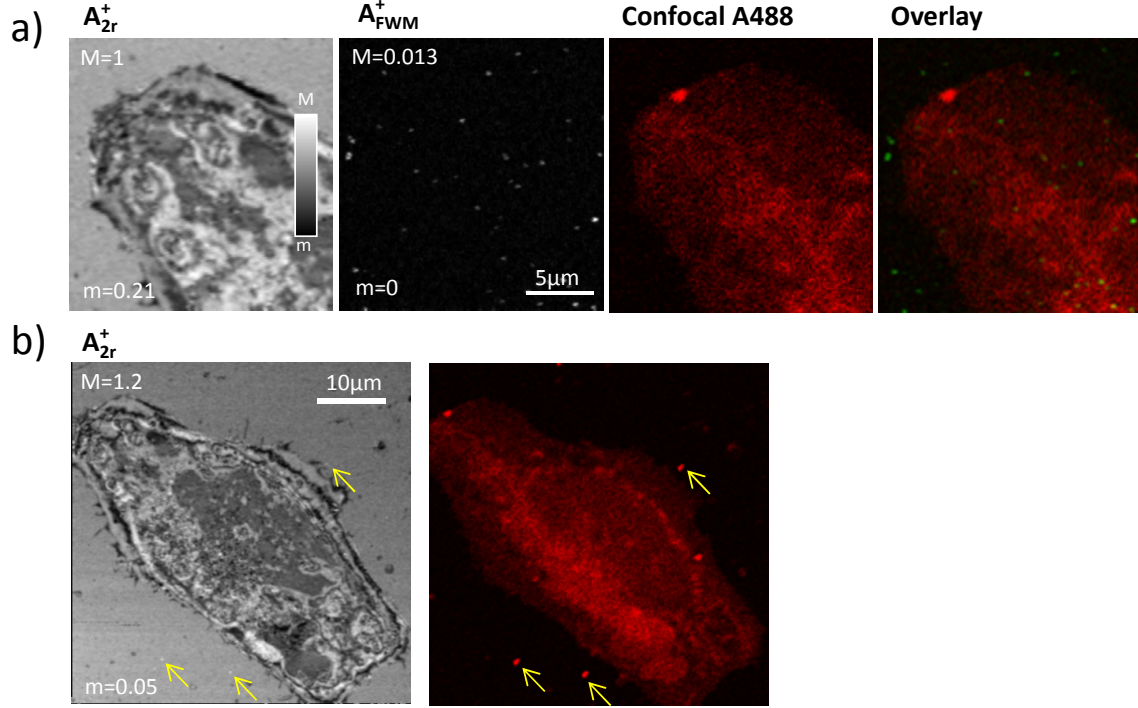


FIG. S9. Fixed HeLa cells that have internalized 15nmAuNP-PC-Tf(A488) at a lower density (factor 0.33) compared to Fig. 4, fixed without washing the NPs after 2 hours incubation (see text). Reflection amplitude ( $A_{2r}^+$ ), FWM amplitude ( $A_{FWM}^+$ ), confocal fluorescence microscopy of the A488 label and overlay (fluorescence (red), FWM amplitude (green)) are shown. FWM was acquired with a pump-probe delay time of 0.5 ps, pump (probe) power at the sample of  $31 \mu\text{W}$  ( $16 \mu\text{W}$ ), 1 ms-pixel dwell time, pixel size in plane of 94 nm and z stacks over  $2.4 \mu\text{m}$  in 300 nm z steps, and is shown as maximum intensity projection. Fluorescence and reflection are on a single plane near the surface. Grey scales are linear from m to M for field amplitudes, as indicated (M=1 corresponds to 5.7mV rms detected by the lock-in). Confocal fluorescence of the Alexa488 shown in a) is not background subtracted and is scaled from 0 to 0.16 of its maximum, to emphasize low values of fluorescence intensity. In b) arrows indicate the location of fluorescent polystyrene beads used as fiducials.

#### **S4. AUTOFLUORESCENCE IN 3T3-L1 CELLS**

Fig.S10 shows an example of 3T3-L1 cells loaded with an unlabeled 20nmAuNP-PC-Ab construct, as control samples for the results in Fig. 5. Images are acquired with the same microscope as in Fig.5 under the same excitation conditions. Regions A and C show the plane near the glass surface (as determined via the reflected field amplitude), while B is a selected plane inside the cell. The fluorescence grey scale is shown using the same intensity value  $F$  (equal to  $2 \times 10^6$  photoelectron/s) as in Fig.5 for direct comparison.

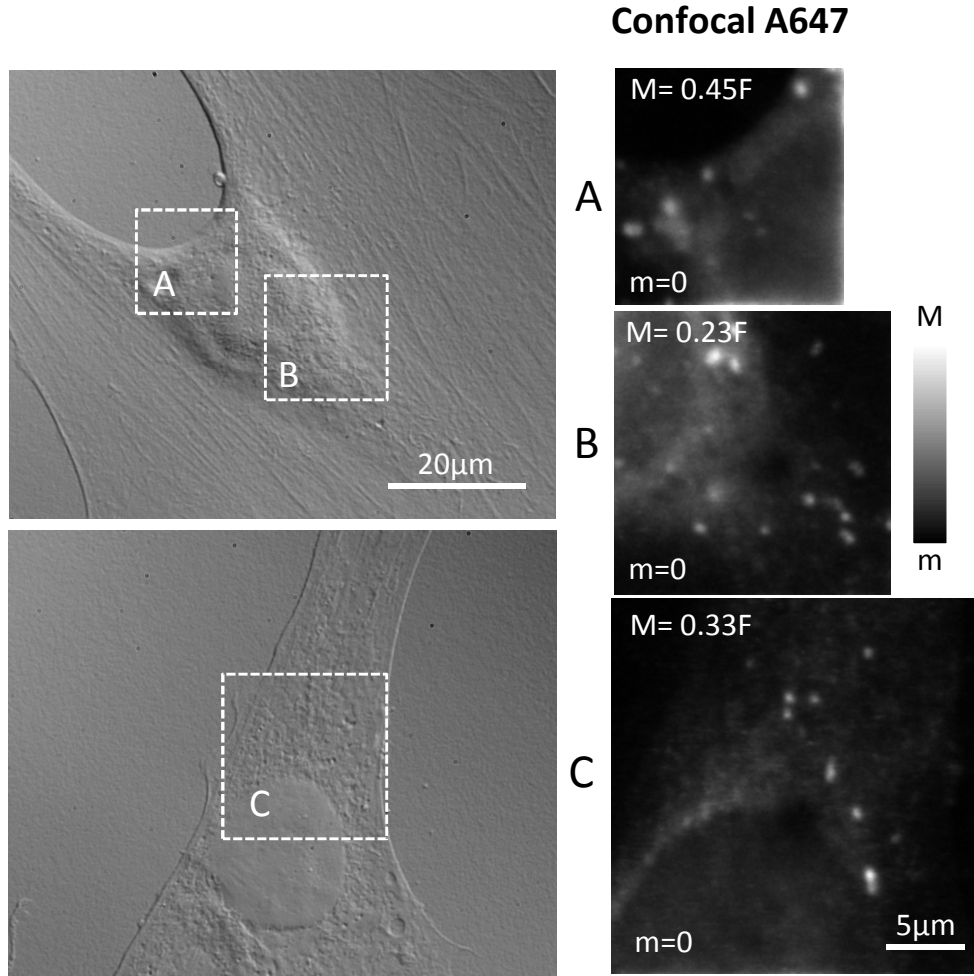


FIG. S10. Fixed 3T3-L1 cells that have internalized unlabelled 20nmAuNP-PC-Ab imaged by differential interference contrast microscopy (left) and confocal fluorescence microscopy (right) of the regions highlighted in DIC. Pump (probe) power at the sample was  $62 \mu\text{W}$  ( $31 \mu\text{W}$ ). The pixel dwell time was 1 ms. Pixel size in plane was 45 nm for A and C, and 62 nm for B. Fluorescence is shown on a single  $x,y$  plane, at the glass substrate interface for A and C, and on a selected plane inside the cell for B. Grey scales are linear from  $m$  to  $M$ , as indicated. The intensity value  $F$  (equal to  $2 \times 10^6$  photoelectron/s) is the same as in Fig. 5 for direct comparison.

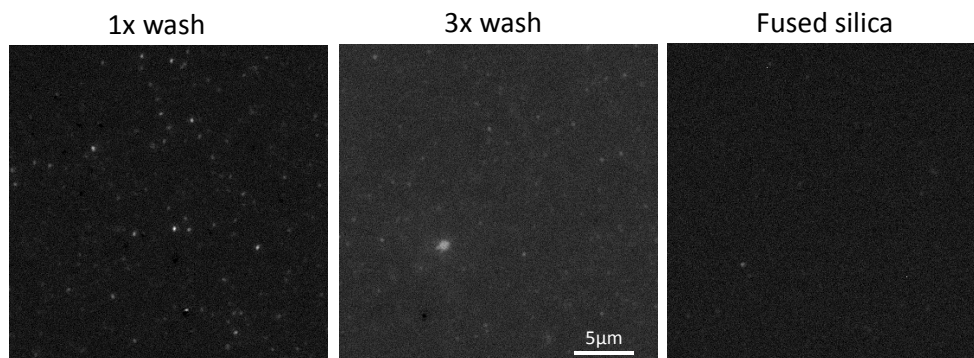


FIG. S11. Fluorescence measured on 10nmAuNP-SA(A488) deposited onto a fused silica coverslip in air. The left and center images are the same images as in Fig. 3. The right image shows the results on a fused silica coverslip without 10nmAuNP-SA(A488). All images are on the same grey scale as in Fig. 3.

## S5. AUTOFLUORESCENCE OF FUSED SILICA AND GLASS COVERSGLIPS

To assess whether the measured fluorescence on the 10nmAuNP-SA(A488) deposited onto fused silica coverslips in Fig. 3 is indeed originating from the Alexa488 fluorophore distinguished from the autofluorescence background, we performed a control experiment on a cleaned fused silica-only coverslip without deposition of the 10nmAuNP-SA(A488) solution, imaged as in Fig. 3. The left and centre images in Fig. S11 show the results in Fig. 3 while the right image is the control, compared on the same intensity grey scale. The cleaned fused silica-only coverslip exhibits almost no punctuated fluorescence, which is therefore originating from the Alexa488 fluorophore after deposition of the 10nmAuNP-SA(A488) solution.

For the 20nmAuNP-PC-Ab(A647) deposited on glass, a glass-only control is shown in Fig. S12 compared on the same intensity grey scale with the results in Fig. 6. In this case, the glass autofluorescence background is negligible compared to the detected fluorescence from the Alexa647.

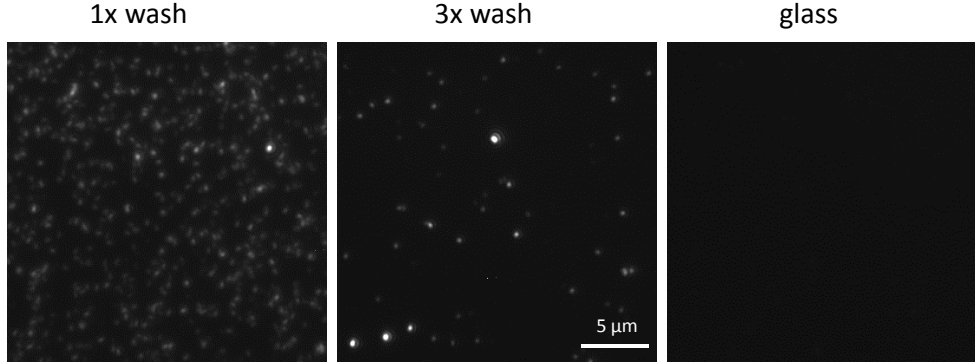


FIG. S12. Fluorescence measured on 20nmAuNP-PC-Ab(A647) deposited onto a glass coverslip in air. The left and center images are the same images as in Fig. 6. The right image shows the results on a glass coverslip without 20nmAuNP-PC-Ab(A647). All images are plotted on the same grey scale, which is the one used in Fig. 6 for the 1x washed sample.

## S6. FULL FIELD OF VIEW IMAGES OF EXTINCTION AND WIDE-FIELD FLUORESCENCE MICROSCOPY

Fig. 3 shows a zoom onto a sub-region corresponding to about 30% of the imaged FOV. The entire FOV for both extinction and fluorescence images is shown in Fig. S13 for the 1× washed sample, and in Fig. S14 for the 3× washed sample, with the ten representative AuNPs used to calculate the cross-section shown in Fig. 3 indicated by arrows and numbers. Images are shown on the same grey scales as in Fig. 3. In this sample, 60 nm diameter AuNPs were added as fiducials to aid finding the focal plane. These are visible as some of the features exhibiting large extinction contrast in Fig. S13 and Fig. S14.

Fig. 6 shows a zoom onto a sub-region corresponding to about 30% of the imaged FOV. The entire FOV for both extinction and fluorescence images is shown in Fig. S15 for the 1× washed sample, and in Fig. S16 for the 3× washed sample, with the ten representative AuNPs used to calculate the cross-section shown in Fig. 6 indicated by arrows and numbers. Images are shown on the same grey scales as in Fig. 3. The co-localisation between AuNPs and Ab(A647) was analysed for Fig. S16 using JACoP, a well documented toolbox for subcellular colocalization analysis under ImageJ [1]. We found that 73% of AuNPs co-localised with fluorescence spots.

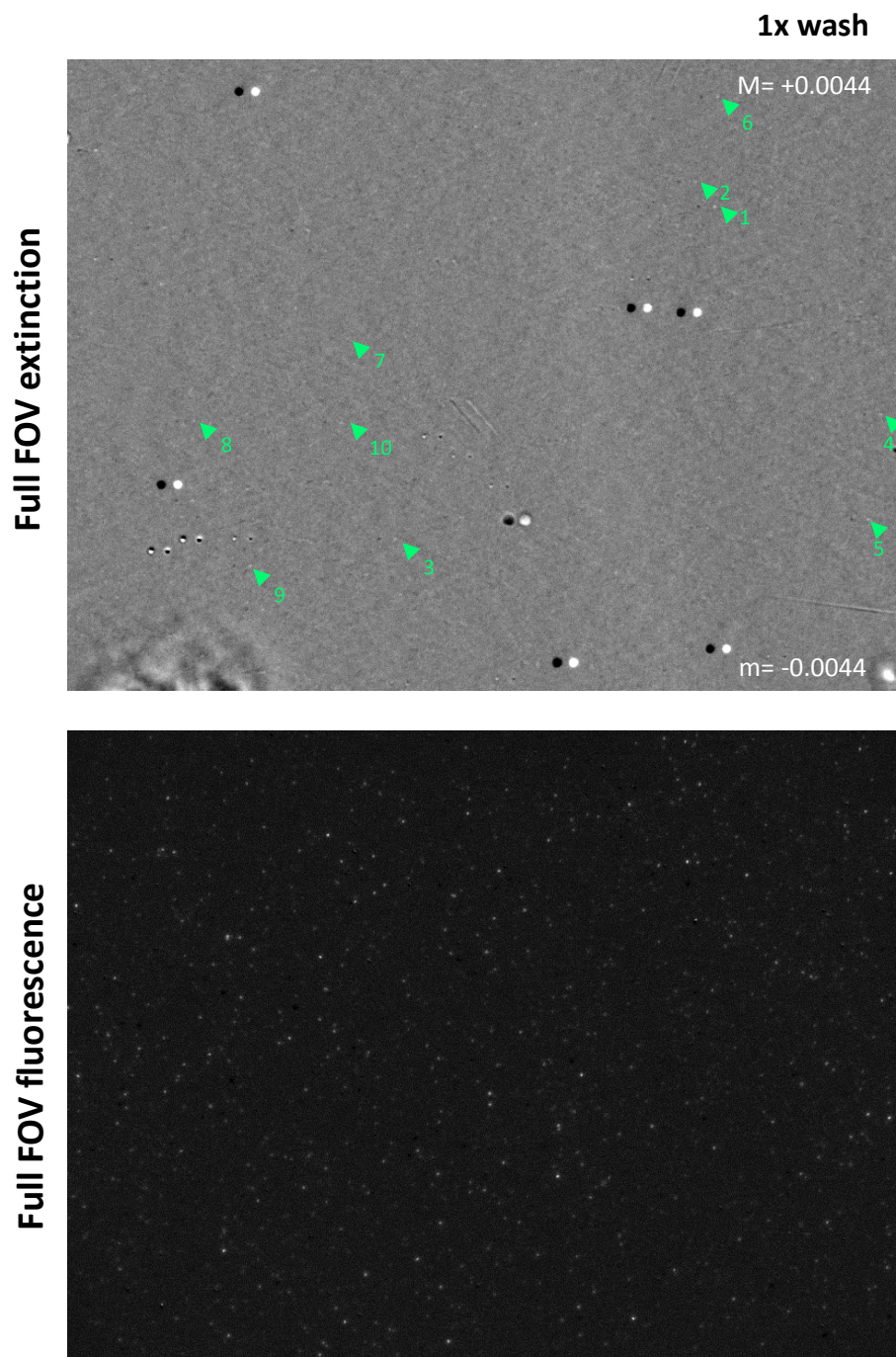


FIG. S13. 10nmAuNP-SA(A488) imaged by correlative extinction microscopy (top) and wide-field fluorescence (bottom), as described in Fig.3 for the  $1\times$  washed sample. Image size is  $96.3\mu\text{m}\times 73.4\mu\text{m}$ . This is the full FOV, of which a portion is shown in Fig.3. The ten representative AuNPs used to calculate the cross-sections plotted in Fig.3 are indicated by arrows and numbers. Images are shown on the same grey scales as in Fig.3.

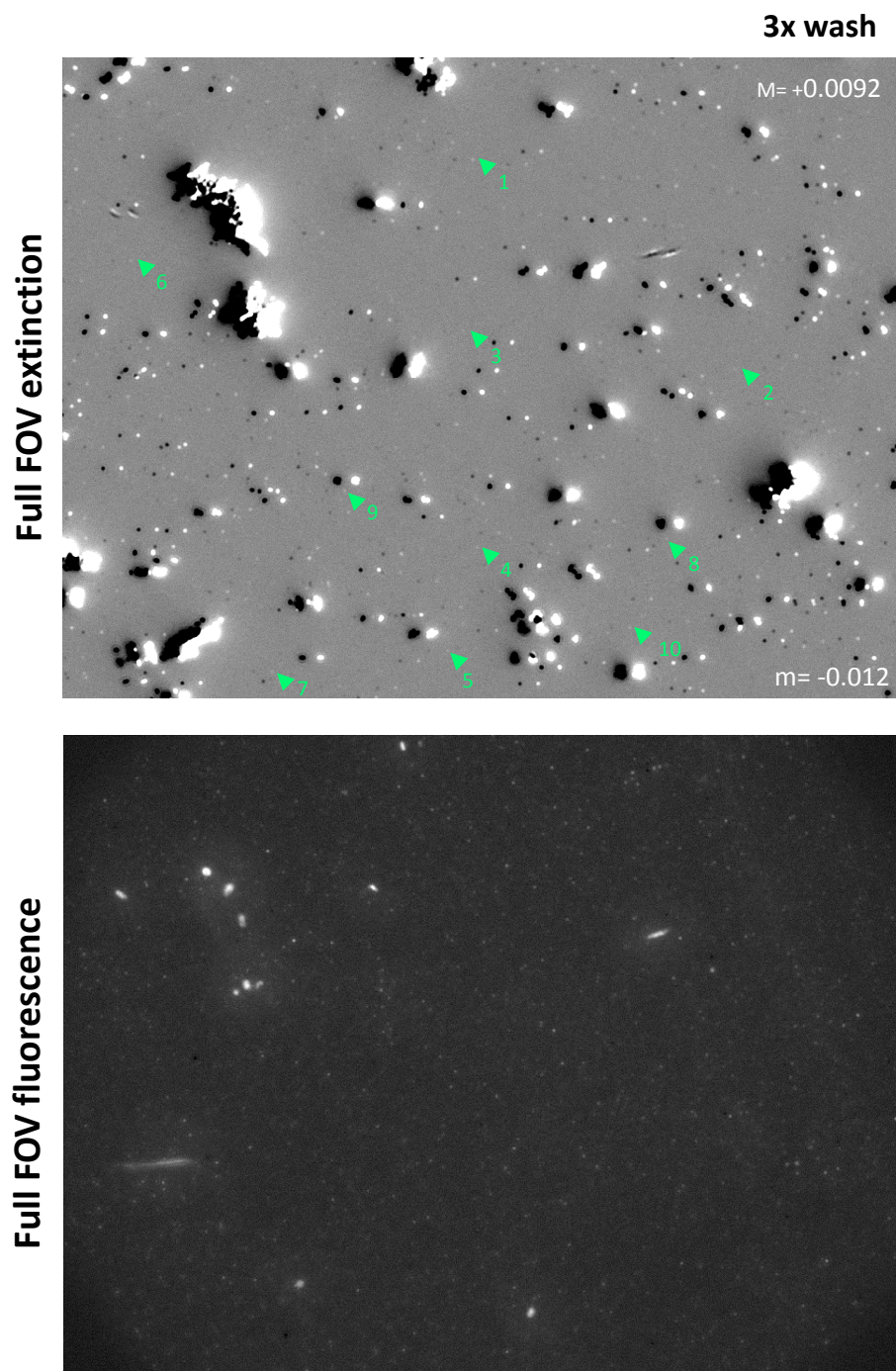


FIG. S14. 10nmAuNP-SA(A488) imaged by correlative extinction microscopy (top) and wide-field fluorescence (bottom), as described in Fig. 3 for the 3 $\times$  washed sample. Image size is  $96.3\mu\text{m}\times 73.4\mu\text{m}$ . This is the full FOV, of which a portion is shown in Fig. 3. The ten representative AuNPs used to calculate the cross-sections plotted in Fig. 3 are indicated by arrows and numbers. Images are shown on the same grey scales as in Fig. 3.

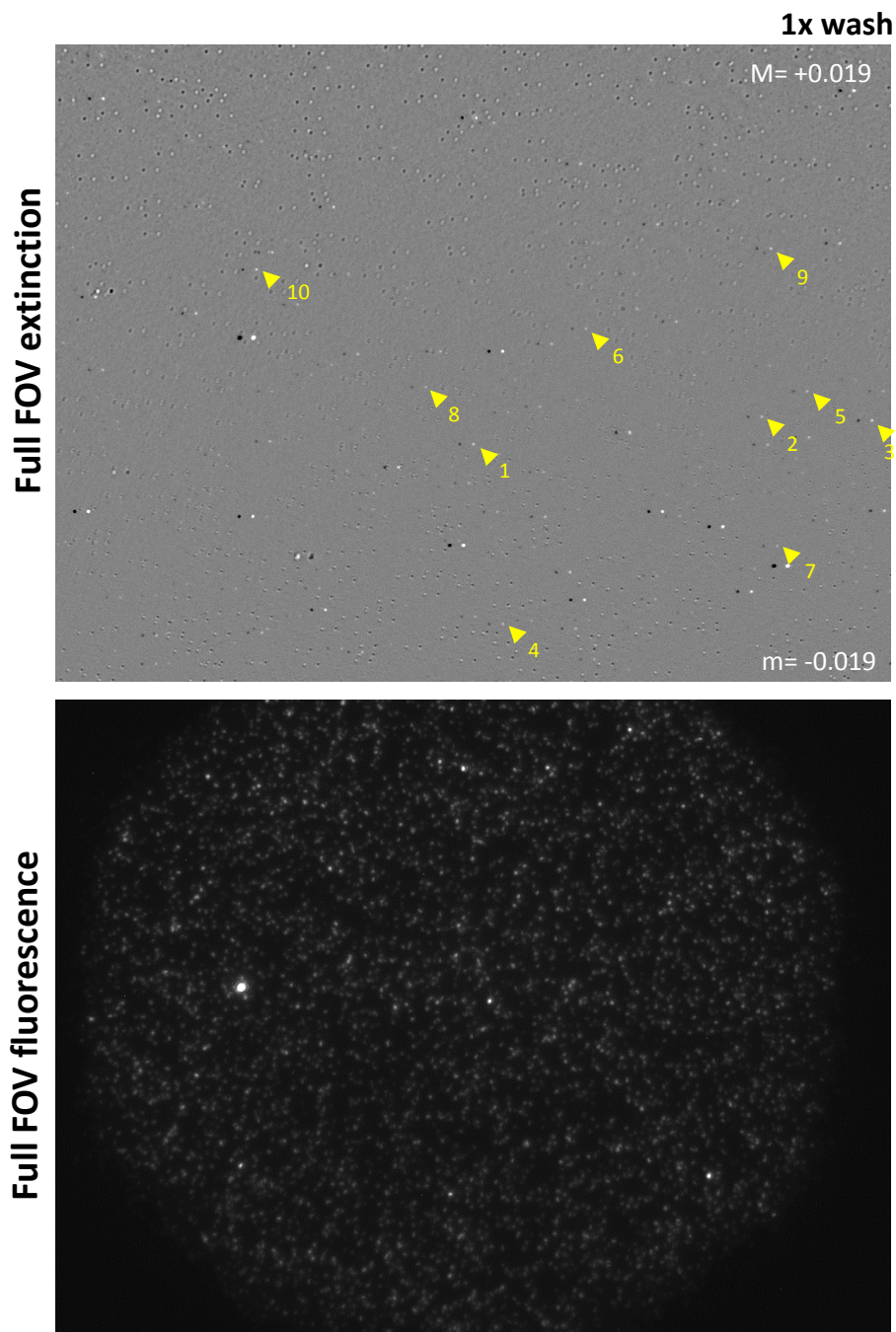


FIG. S15. 20nmAuNP-PC-Ab(A647) imaged by correlative extinction microscopy (top) and wide-field fluorescence (bottom), as described in Fig.6 for the 1 $\times$  washed sample. Image size is 96.3 $\mu\text{m}\times$ 73.4 $\mu\text{m}$ . This is the full FOV, of which a portion is shown in Fig.6. The ten representative AuNPs used to calculate the cross-sections plotted in Fig.6 are indicated by arrows and numbers. Images are shown on the same grey scales as in Fig.6.

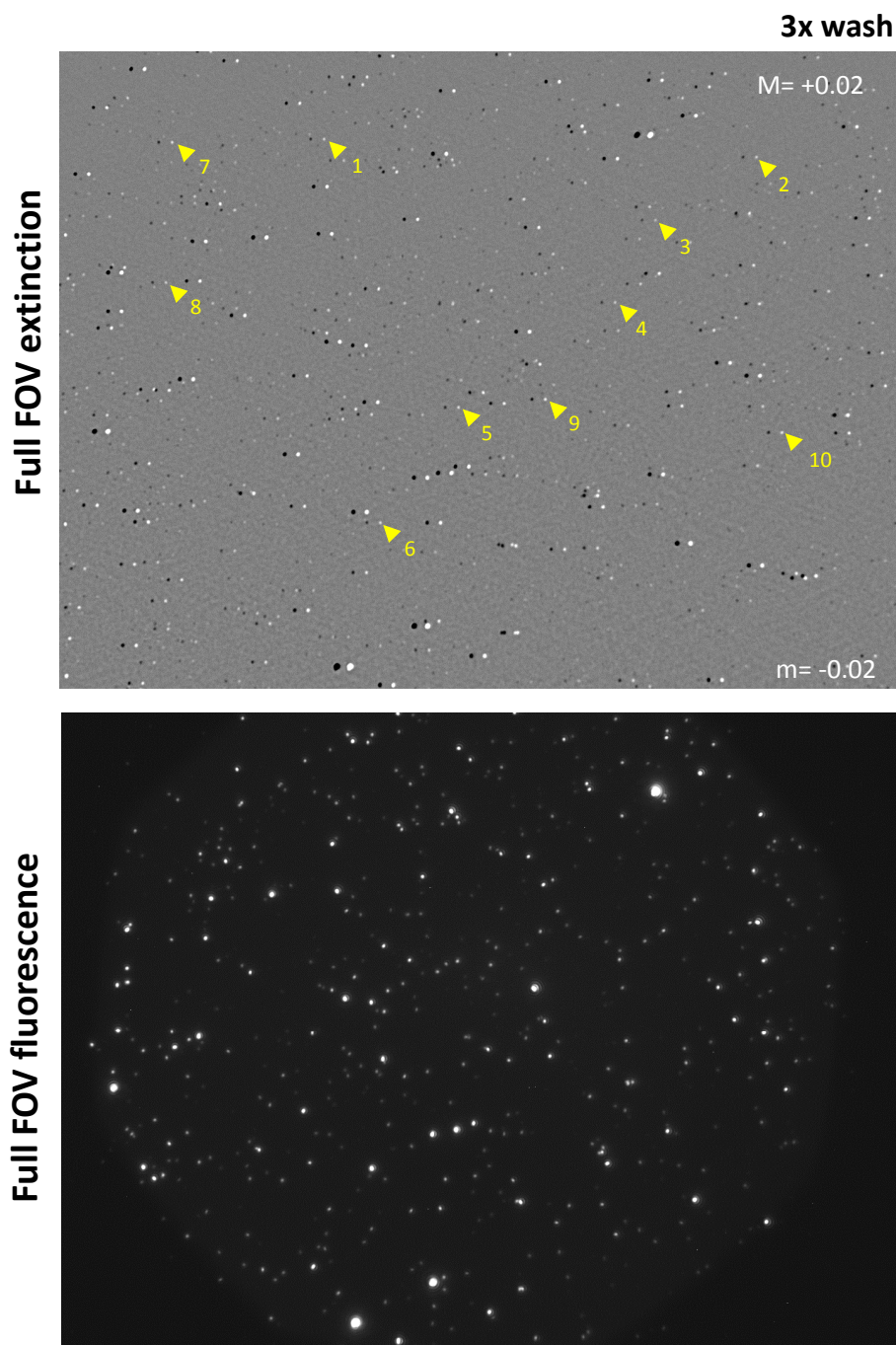


FIG. S16. 20nmAuNP-PC-Ab(A647) imaged by correlative extinction microscopy (top) and wide-field fluorescence (bottom), as described in Fig.6 for the 3 $\times$  washed sample. Image size is  $96.3\mu\text{m} \times 73.4\mu\text{m}$ . This is the full FOV, of which a portion is shown in Fig.6. The ten representative AuNPs used to calculate the cross-sections plotted in Fig.6 are indicated by arrows and numbers. Images are shown on the same grey scales as in Fig.6.

## S7. ANALYSIS OF FLUORESCENCE QUENCHING

In order to estimate the number of fluorescent molecules attached to a AuNP, and the fluorescence quenching by the AuNP, we have analysed the extinction and fluorescence images of the  $3\times$  washed sample 20nmAuNP-PC-Ab(A647), shown in Fig. S16. The analysis was performed using a in-house software implemented in ImageJ’s macro language. Firstly, the two images were registered by a custom pattern-detection algorithm to account for small drifts. Then, particle peaks were identified either in the fluorescence or the extinction data, giving rise to two different sets of particle positions. Extinction cross-sections were calculated, for each set of coordinates, as described by Payne *et al.* [2] using the shifted contrast method. Fluorescence was calculated for each set of coordinates as the integrated emission over an area given by the point-spread function, taken as a circle of radius  $R_i$  equal to 6 pixels, corresponding to 387 nm on the sample, and approximately  $\lambda/\text{NA}$ , with the centre wavelength  $\lambda = 550$  nm and the numerical aperture  $\text{NA} = 1.45$  of the objective used. A local background subtraction was used, based on a double radius method described in our previous work [3]. To enable this subtraction, in the assignment of particle coordinates, a proximity restriction was adopted, namely if two peaks were separated by a distance smaller than  $2R_i$  they were excluded. The integrated fluorescence was quantified as detected photoelectrons per second (pe/s) using the exposure time of 10 s and the camera gain of 4.45 e/count. The measurement noise was found to be 38 pe/s root mean square (RMS) in fluorescence and  $64 \text{ nm}^2$  RMS in extinction.

The resulting fluorescence versus extinction cross-section of the particles is given in Fig. S17. Data points in the image are divided into three groups, namely particles identified in fluorescence only (red squares), extinction only (black squares), or both (blue squares). For the latter, we used the criterion whereby particle positions differing by less than  $R_i$  between the two sets of coordinates were assumed to represent the same particle. From the results in Fig. S17 we can identify a set of single AuNPs having no fluorescence within the measurement noise, with  $\sigma_{\text{ext}}$  in the range of 150 to  $400 \text{ nm}^2$ . The histogram of all particles identified in extinction (bottom right) shows a peak around  $300 \text{ nm}^2$ , and a broader secondary peak around  $600 \text{ nm}^2$ . This suggests that a single AuNP in the sample has on average a measured extinction cross-section of  $300 \text{ nm}^2$ , consistent with expectations taking into account the nominal 20 nm particle diameter and that measurements were performed in

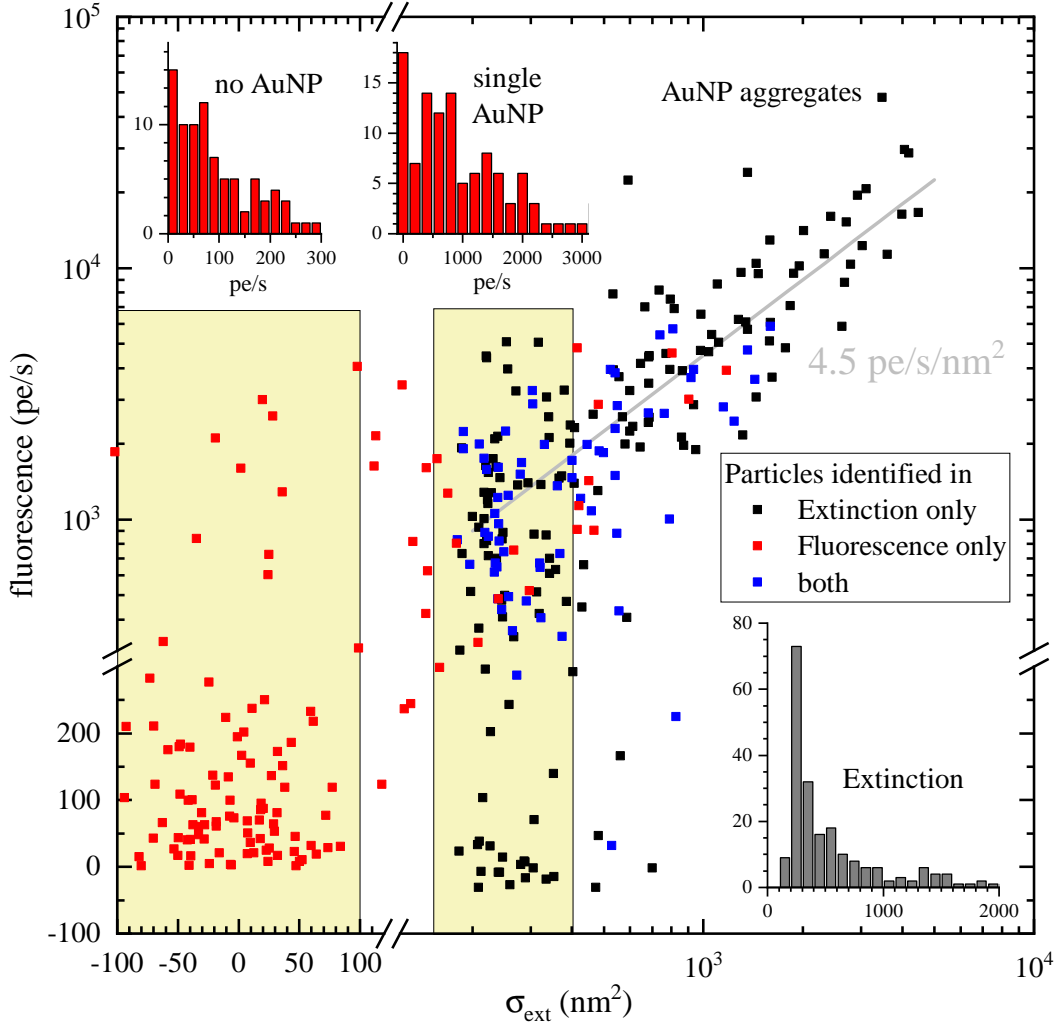


FIG. S17. Analysis of the  $3\times$  washed sample of 20nmAuNP-PC-Ab(A647), using the data shown in Fig. S16. Fluorescence flux (in units of detected photoelectrons/s) versus extinction cross-section of particles identified in fluorescence only (red squares), extinction only (black squares), or both (blue squares). Regions corresponding to no AuNP ( $|\sigma_{\text{ext}}| < 100 \text{ nm}^2$ ) or one AuNP ( $\sigma_{\text{ext}} = 150 - 400 \text{ nm}^2$ ) are indicated, and the associated histograms of fluorescence flux are shown. Additionally, a histogram of the extinction cross-section for all the particles identified in extinction is shown on the right. The grey line indicates a linear scaling of  $4.5 \text{ pe/s/nm}^2$ .

air, resulting in a reduction of  $\sigma_{\text{ext}}$  compared to particles in a high refractive index medium. For larger  $\sigma_{\text{ext}}$  values corresponding to multiple AuNPs, likely aggregates within the diffraction limited resolution, we observe that the fluorescence is proportionally increasing, scaling as  $4.5 \text{ pe/s/nm}^2$  with  $\sigma_{\text{ext}}$ , as we would expect when the fluorescence is originating from fluorophores attached to the AuNPs. Taking  $300 \text{ nm}^2$  as the typical cross-section for a single AuNP, we then deduce a fluorescence of  $1350 \text{ pe/s}$  per AuNP. The histogram of the measured fluorescence for single AuNPs ( $\sigma_{\text{ext}} = 150 - 400 \text{ nm}^2$ ) is shown in Fig. S17 top middle. Although the distribution is quite wide, it is consistent with a value of  $1350 \text{ pe/s}$  per AuNP.

Fluorophores not bound to AuNPs are seen in Fig. S17 as fluorescent particles with a  $\sigma_{\text{ext}}$  within the noise – we use here a  $\sigma_{\text{ext}}$  range of  $\pm 100 \text{ nm}^2$ . The resulting fluorescence histogram is shown on the top left, and reveals a wide distribution of intensities. This can be expected due to the random bleaching within the 10 s exposure, and the random orientation of the linear dipole of the fluorophore relative to the axial direction, which affects excitation and collection efficiencies in epi-fluorescence [4]. We estimate an average single fluorophore flux of about  $100 \text{ pe/s}$  from this histogram.

Fluorophores close to AuNPs can be quenched due to Förster-transfer, or in other words emission into surface plasmons of the AuNP which are mostly absorbed as opposed to radiated to the far-field. This effect has been studied over the last decade, with two works [5, 6] specifically relevant to the present study. In the latter,  $20 \text{ nm}$  AuNPs and the fluorophore Alexa647 were used, matching our experiment. It was found that when the dye is at a distance of  $5 \text{ nm}$  from the gold surface, the fluorescence is reduced to about 10% relative to free space (see Fig. 3a in [6]). The  $20 \text{ nm AuNP-PC-Ab(A647)}$  construct is specified by the manufacturer to have a polymer shell of  $2 \text{ nm}$  thickness when measured in electron microscopy under dry conditions. In water, the polymer is hydrated and the the shell thickness will increase. In addition, the Alexa647 dye is attached to the polymer shell via an antibody, adding further separation to the AuNP. Assuming therefore an average  $5 \text{ nm}$  distance between the dye and the AuNP in our sample, we can estimate  $10 \text{ pe/s}$  fluorescence flux from a single fluorophore bound to a AuNP, and thus about 135 fluorophores per AuNP in average from the above determined value of  $1350 \text{ pe/s}$  per AuNP. We note that at  $15 \text{ nm}$  radius ( $10 \text{ nm}$  NP radius plus  $5 \text{ nm}$  distance), the surface area is  $2827 \text{ nm}^2$ , and thus  $21 \text{ nm}^2$  per fluorophore, corresponding to an average fluorophore separation of about  $5 \text{ nm}$ ,

a reasonable surface coverage taking into account the few nm size of the antibody.

---

- [1] Bolte, S. & Cordèlières, F. P. A guided tour into subcellular colocalization analysis in light microscopy. *Journal of Microscopy* **224**, 213–232 (2006).
- [2] Payne, L. M., Langbein, W. & Borri, P. Wide-field imaging of single-nanoparticle extinction with sub-nm<sup>2</sup> sensitivity. *Phys. Rev. Applied* **9**, 034006 (2018).
- [3] Payne, L. M., Langbein, W. & Borri, P. Polarization-resolved extinction and scattering cross-section of individual gold nanoparticles measured by wide-field microscopy on a large ensemble. *Appl. Phys. Lett.* **102**, 131107–1 (2013).
- [4] Anger, P., Bharadwaj, P. & Novotny, L. Enhancement and quenching of single-molecule fluorescence. *Physical Review Letters* **96**, 113002 (2006).
- [5] Reineck, P. *et al.* Distance and wavelength dependent quenching of molecular fluorescence by au@SiO<sub>2</sub> core-shell nanoparticles. *ACS Nano* **7**, 6636–6648 (2013).
- [6] Holzmeister, P. *et al.* Quantum yield and excitation rate of single molecules close to metallic nanostructures. *Nat. Commun.* **5**, 5356 (2014).